IEEE Access
Multidisciplinary ⋮ Rapid Review ⋮ Open Access Journal

Received 16 March 2024, accepted 2 April 2024, date of publication 12 April 2024, date of current version 29 April 2024.

Digital Object Identifier 10.1109/ACCESS.2024.3388252

RESEARCH ARTICLE

An Improved Model-Free Predictive Current Control for PMSM Drives Based on Current Circle Tracking Under Low-Speed Conditions

YIQI FENG[1], CHENGNING ZHANG[1], SHENGPING HUANG[2], SHUO ZHANG[1], (Member, IEEE), JIANZHEN QU[3], (Member, IEEE), ZHAOZONG LI[1], (Member, IEEE), LI ZHAI[1], (Member, IEEE), AND YUE ZHAO[1]

[1]National Engineering Laboratory for Electric Vehicles, School of Mechanical Engineering, Beijing Institute of Technology, Beijing 100081, China
[2]Jianglu Machinery Electronics Group Company Ltd., Xiangtan 411199, China
[3]Department of Electrical Engineering, Tsinghua University, Beijing 100084, China

Corresponding author: Shuo Zhang (shuozhangxd@gmail.com)

This work was supported by the National Key Research and Development Program of China under Grant 2021YFB2500603.

ABSTRACT The model predictive current control (MPCC) method for permanent magnet synchronous motor (PMSM) has been widely applied due to its quick current response. However, the performance of MPCC relies on the real-time model accuracy deeply. Meanwhile, the large stator current harmonic under low-speed conditions is another defect of MPCC. To solve these problems, an improved model-free predictive current control method based on online data-driven, and a novel modulation method based on current increment synthesis are proposed in this paper. Firstly, the unknown polynomial related to PMSM parameters (regarding resistance, inductance, and flux-linkage) is defined as a lumped term in the MPCC model. The stator current and voltage measurements in the latest 15 sampling periods are registered as a database by the rolling update mechanism, and used to identify the unknown lumped term. Secondly, according to the identified result, the current increments corresponding to each active voltage in the next sampling period are updated online. Finally, the duty cycle of the inverter at the next sampling period is calculated based on the minimization of the predicted current increment tracking error. The effectiveness and real-time implementation of the proposed method are verified by experiments under different working conditions.

INDEX TERMS Model-free predictive current control, current increment modulation, surface-mounted permanent magnet synchronous machine.

NOMENCLATURE

i_s, U_s	Motor stator current and voltage value.
u_d, u_q, i_d, i_q	Motor voltage and current in *dq-axis*.
U_{dc}	Voltage of the DC power supply.
R_s, R_s'	Actual and rated stator resistance.
L_s, L_s'	Actual and rated stator inductance.
L_d, L_q	Motor stator inductance in *dq-axis*.
ψ_r, ψ_r'	Actual and rated PM flux.
ω_m, ω_e	Mechanical and electrical angular velocity.
θ_e, θ_r	Rotor electrical angle and position.
p_n	The number of pole pairs.
T_e, T_L	Electromagnetic torque and Load Torque.
T_s, T_k	Sampling period and sampling time.

The associate editor coordinating the review of this manuscript and approving it for publication was Alfeu J. Sguarezi Filho.

I. INTRODUCTION

The permanent magnet synchronous motor (PMSM) has been widely used in electric vehicles, electric aircraft, and other

servo systems due to its high efficiency and high power density [1], [2]. The control algorithm plays a significant role in the enhancement of stator current control performance for PMSM drives. With the development of microprocessors, more sophisticated control algorithms could be implemented on the PMSM drives [6].

Among these sophisticated control techniques, the model predictive control (MPC) has become a research hotspot. The advantages of using MPC in PMSM drives are from the following aspects: 1) designing and introducing mathematical models can predict the future behavior of the system accurately; 2) Modern microprocessors can solve massive real-time computations with a better time cost performance; 3) The control logic of MPC is convenient to understand and implement, and can realize multi-objective optimization with constraints [3], [4], [5].

Despite the above advantages, there are still some critical challenges that need to be solved: 1) The predicted accuracy of MPC is deeply dependent on the real-time accuracy of the PMSM's prediction model; 2) The modulation process of classical MPC leads large modulation error and current harmonic, particularly as the system is operating under low-speed conditions [6], [7], [8], [9]. Generally, the actual value of motor parameters is hard to detect in real time due to the expensive sensor cost and limited motor manufacturing technology [10], [11]. Furthermore, the modulation error of MPC can be reduced by a higher switching frequency in practical applications. However, these measures require high purchase costs, which is not conducive to the widespread application of MPC in PMSM drives. It should be noted that the defects of MPC mentioned above can also be solved by suitable control algorithms deployed on modern microprocessors.

To overcome the model dependency of MPC, many kinds of control methods have been proposed. Overall, they can be divided into the following categories: 1) Parameters online identification algorithm; 2) Compensation algorithm with disturbance observer; 3) Model-free control method, etc. [7]. The Kalman Filter (KF) [12], [13], [14], [15] is the typical solution in online parameter identification technologies and has been widely used in different area. However, its filtering accuracy is quite sensitive to the initial settings of the noise covariance matrix, which makes it only suitable for deployment on the AC motor that runs at constant working point. Moreover, the Kalman Filter algorithm is usually designed to identify one or two parameters simultaneously to avoid the excessive instantaneous computational burden.

Another method to deal with the model dependency of MPC is to treat the disturbances caused by motor parameter mismatching as a variable term in the predictive model [16], [17], [18]. This variable term is identified as well as compensated online by designing different kinds of observer algorithms [19], [20], [21], [22], [23], [24]. Wang et al. [24] proposed an inductance parameter estimation method to ensure the robustness of observer with a smaller estimated burden. However, the robustness of such methods can only be ensured by sacrificing the optimal control performance and the parameters of observer need to be adjusted carefully also [7].

As an emerging control concept, the model-free control method [25] has received extensive attention for it is completely independent of the motor parameters, but it still needs to establish a mathematical model for predicted controlling. The proportional-integral (PI) control is one of the well-known model-free control methods [26]. However, the gain parameters of the PID controller need to be testified by experiments and set carefully [27]. The ideal solution of model-free control is to identify all kinds of disturbances under all operating conditions and store them in high-resolution look-up tables (LUT) [28]. However, due to manufacturing deviations, environmental temperature change, material aging, etc, it is unrealistic to measure and store all kinds of disturbances in offline LUTs. [29].

Currently, in the area of model-free predictive current control (MFPCC) for PMSM drives, the stator current and voltage measurements in the latest sample period are defined as input signals of the model-free control algorithm [30]. Then, the algorithm calculates the optimal switch states of the inverter at next sample period based on storage data. By this way, the model-free control requires less random access memory (RAM) space than LUTs [31]. However, the main defects of MFPCC is the stator current harmonic and torque ripple caused by stagnant current update mechanism and single-voltage vector modulation [32], [33], [34]. To get rid of the stagnant current update mechanism, Ma et al. [32], and Yu et al. [33] proposed a novel current updated mechanism. The switch state that has not been conducted during the latest 50 sample periods is forced to conduct at the next period, even though it may not be the optimal switch state. Yuan et al. [34] improved the algorithm mentioned above with a new anti-stagnant current update mechanism. However, its optimum control performance can only be obtained under a high switching frequency (30kHz).

To suppress the stator current harmonic under low-speed steady-state conditions of MPCC, the multi-vector synthesis modulation has been proposed and testified in previous research. Wang et al. [35] proposed a multistep MPC to decrease the phase current harmonics under the steady-state conditions. Zhou et al. [36] developed a novel multi-vector synthesis modulation method with two adjacent voltage vectors and a zero voltage vector. Sun et al. [37] proposed a new modulation method, which applies an active-current increment vector and a negative current increment to synthesize the optimal current increment vector.

According to the literature review above, it can be concluded that the present parameter identification and disturbance compensation for MPCC in PMSM drive are limited due to the heavy computational burden and sensitiveness of algorithm coefficients initial setting. The existing model-free control algorithm still needs to deploy under high switching frequency to overcome the stagnant current updated

mechanism. Moreover, the modulation process based on optimal voltage vector synthesis ignores the effect of negative current increment that generated by the zero voltage vector. And, there is no suitable modulation method for suppressing stator current harmonics under low-speed steady-state conditions yet.

To overcome such drawbacks, the motivation of this paper is to propose a model-free predictive current control based on online data-driven with less RAM space requirement and lower calculation burden, which aims to improve the current prediction accuracy of MPCC without using any motor parameters. Moreover, a novel modulation based on the stator current increment synthesis is proposed to suppress the current harmonic under low-speed steady-state working conditions.

The contributions of this article are described as follows:

1) An improved model-free predictive current control method driven by online data is proposed to overcome the real-time model dependency of MPCC without using motor parameters;
2) A rolling online data update mechanism with variable-time window is proposed to calculate the unknown lumped polynomial that related to the PMSM parameters by less random access memory space requirement and lower computational burden;
3) A novel modulation method based on an anti-stagnant current update mechanism and reference stator current increment synthesis is proposed to reduce the current harmonics under low-speed steady-state conditions;

The structure of this paper is organized as follows. Section II introduces the control logic of the classical MPCC. The proposed model-free predictive current control is presented in Section III. The proposed modulation method is described in Section IV. Section V discussed the experimental results. Section VI concludes the whole paper.

II. CLASSICAL MPCC FOR SPMSM

A. THE CONTINUOUS-TIME MODEL OF PMSM

Some assumptions should be declared before establishing the PMSM mathematical model [34].

1) The PMSM has symmetrical three-phase winding.
2) The magnetomotive force of the PMSM is with sinusoidal distribution along the air gap.
3) The eddy current, hysteresis, and core losses of PMSM are ignored.
4) In Surface-mounted PMSM (SPMSM), $L_d = L_q = L_s$.

Therefore, the PMSM's continuous-time model can be expressed as [34]

$$U_s = R_s i_s + L_s \cdot \left(di_s / dt\right) + j\psi_r \omega_e e^{j\theta_e} \tag{1}$$

B. THE CONTROL LOGIC OF CLASSICAL MPCC

The classical MPCC could predict the current behaviors at the end of next sampling period with different inverter switching states and select the optimal switching state based on the cost function. Since the discrete operating characteristics of the IGBTs, the continuous-time model of PMSM needs to be transformed into a discrete state equation by the first-order Euler discretization. The predicted stator current at $(k+1)$th instant can be obtained as

$$i_s^{pre}(k+1) = i_s(k) + \frac{T_s}{L_s'}\left[u_s(k) - R_s' i_s(k) - j\psi_r' \omega_e(k) e^{j\theta_e(k)}\right] \tag{2}$$

where $u_s(k)$ represents the optimal stator voltage vector in the (k)th sampling period, which is calculated at $(k-1)$th period and outputs by inverter at the beginning of the (k)th sampling period.

Due to the one-step delay by the digital system, the one-step compensation should be taken into account in the calculation process of MPCC. Since the mechanical frequency is much smaller than the electric frequency in the PMSM drives, it can be regarded that $\omega_e(k+1) = \omega_e(k)$ and $\theta_e(k+1) = \theta_e(k)$ between the adjacent sampling period under low-speed conditions. The predicted current at $(k+2)$th instant can be obtained as

$$\begin{aligned} i_{si}^{pre}(k+2) &= i_s^{pre}(k+1) + \frac{T_s}{L_s'}\left[u_s(k+1)_w - R_s' i_s(k+1)\right. \\ &\quad \left. - j\psi_r' \omega_e(k+1) e^{j\theta_e(k+1)}\right]; w \in \{0,1,2,3,4,5,6,7\} \end{aligned} \tag{3}$$

where $u_{si}(k+1)$ represents the candidate stator voltage vector in the $(k+1)$th sampling period. The w indicates the eight candidate voltage vector control set, which corresponds to eight switching states of inverter, including (000), (100), (110), (010), (011), (001), (101), (111).

The cost function defined as Eq.(4) is used to compare the tracking error between the reference current $i_s^{ref}(k+2)$ and prediction current $i_s^{pre}(k+2)_w$ with the defined control set above [6]. Finally, the optimal voltage vector in the $(k+1)$th sampling period is selected based on the minimization of the cost function and applied in the $(k+1)$th sampling period.

$$J_i = \left| i_s^{ref}(k+2) - i_s^{pre}(k+2)_w \right|, w \in \{0,1,2,3,4,5,6,7\} \tag{4}$$

According to the description above, the control scheme of classic MPCC and the time sequence of the stator current predictive process can be demonstrated in Fig.1. Moreover, the stator current sampling time T_k is set as 0.1μs in this paper.

III. THE IMPROVED MODEL-FREE PREDICTIVE CURRENT CONTROL METHOD

To overcome the model dependency, an improved model-free predictive current control algorithm is proposed without using motor parameters. Its process is described as follows.

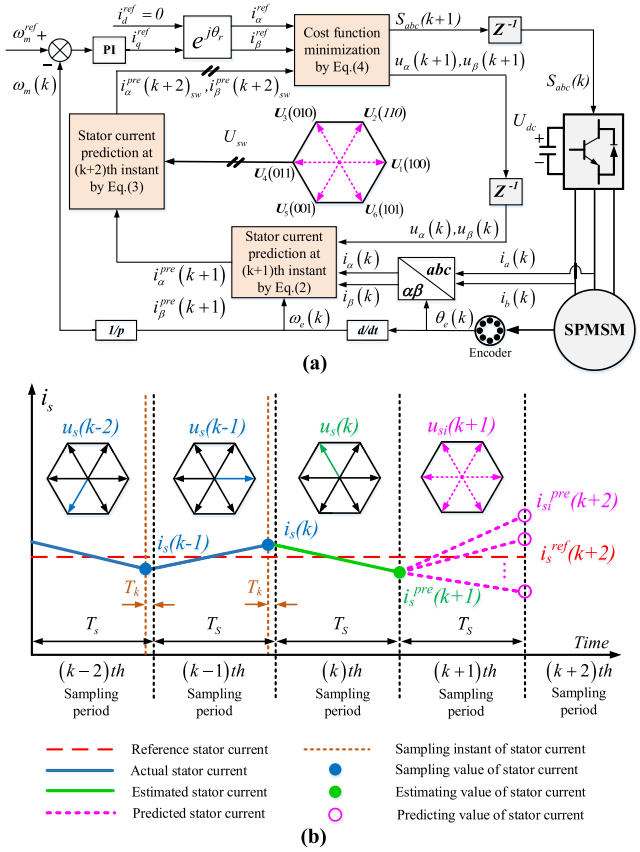

FIGURE 1. The demonstration of classic MPCC. (a) Control scheme of classic MPCC; (b) Time sequence of stator current predictive process.

A. THE NONPARAMETRIC MATHEMATICAL MODEL OF SPMSM

The continuous-time stator current differential model of SPMSM under the *dq-axis* could be expressed as

$$\begin{cases} \dfrac{di_d}{dt} = \dfrac{1}{L_s}\left(u_d - R_s i_d + \omega_e L_s i_q - U_{d-par}\right) \\ \dfrac{di_q}{dt} = \dfrac{1}{L_s}\left[u_q - R_s i_q - \omega_e\left(L_s i_d + \psi_r\right) - U_{q-par}\right] \end{cases} \tag{5}$$

where terms U_{d-par}, U_{q-par} represent the voltage disturbance caused by the motor parameter mismatching.

Based on the Eq.(5), the continuous-time nonparametric stator current differential model can be re-written as

$$\frac{di_d}{dt} = \underbrace{\left(u_d - R_s i_d + \omega_e L_s i_q - U_{d,par}\right)/L_s - c_d u_d}_{X_d} + c_d u_d$$

$$\frac{di_q}{dt} = \underbrace{\left[u_q - R_s i_q - \omega_e\left(L_s i_d + \psi_r\right) - U_{q,par}\right]/L_s - c_q u_q}_{X_q} + c_q u_q$$

In matrix form, it can be expressed as

$$di_{dq}/dt = X_{dq} + c_{dq} \cdot u_{dq} \tag{6}$$

where $i_{dq} = \begin{bmatrix} i_d \\ i_q \end{bmatrix}, X_{dq} = \begin{bmatrix} X_d \\ X_q \end{bmatrix}, c_{dq} = \begin{bmatrix} c_d & 0 \\ 0 & c_q \end{bmatrix}, u_{dq} = \begin{bmatrix} u_d \\ u_q \end{bmatrix}$. The i_{dq} and u_{dq} represents the stator current and voltage measurements. The X_{dq} represents the unknown lumped polynomial that related to motor parameters. The coefficient c_d, c_q represents the scaling factors of u_d, u_q and set to $(1/L_s)$ commonly.

According to the first-order Euler discretization, the discrete-time formula of Eq.(6) can be obtained as

$$i_{dq}(k+1) = i_{dq}(k) + \left[X_{dq}(k) + c_{dq} \cdot u_{dq}(k)\right] \cdot T_s \tag{7}$$

B. THE UNKNOWN POLYNOMIAL CALCULATION BASED ON DATA-DRIVEN

Due to its time-variable feature and the undetectable characteristic, the X_{dq} in Eq.(7) needs to be treated as a constant value during each sampling period, which could be expressed as $\hat{X}_{dq}(k) = \left[\hat{X}_d(k), \hat{X}_q(k)\right]^T$. Therefore, the Eq.(6) can be treated as an ultra-local model [25] and expressed as

$$d\left(i_{dq}\right)/dt = \hat{X}_{dq} + c_{dq} \cdot u_{dq} \tag{8}$$

where $\hat{X}_{dq}$ is the calculated value of the unknown term X_{dq}. In this paper, the discrete-time domain calculation of the $\hat{X}_{dq}$ in $[t-\Gamma, t]$ time domain could be obtained by using the algebraic parameter identification techniques [38] as

$$\hat{X}_{dq} = -\frac{3!}{\Gamma^3}\int_0^{\Gamma}\left[(\Gamma - 2\sigma)\, i_{dq}(\sigma) + x_{dq} \cdot \sigma\,(\Gamma - \sigma)\, u_{dq}(\sigma)\right]d\sigma \tag{9}$$

where Γ is the $[t-\Gamma, t]$ variable-time window for data storage, which is longer than n_T sampling periods and is defined as $\Gamma \geq n_T \cdot T_s$. The Γ and n_T are both set as a positive integer. Since the high sampling frequency characteristic in the PMSM control algorithm, the numerical solution of the integrator in Eq.(9) can be approximately deduced from the complex trapezoidal formula. The discrete-time calculation of $\hat{X}_{dq}$ at (k)th sampling period for digital process implementation could be expressed as

$$\begin{aligned} \hat{X}_{dq}(k) = -\frac{3}{n_T^3 \cdot \Gamma}\sum_{\delta=1}^{n_T}\Big(&\left(n_T - 2(\delta-1)\right) \cdot i_{dq}[\delta-1] \\ &+ c_{dq} \cdot \Gamma \cdot (\delta-1) \cdot \left(n_T - (\delta-1)\right) \cdot u_{dq}[\delta-1] \\ &+ (\Gamma - 2\delta) \cdot i_{dq}[\delta] + c_{dq} \cdot \delta \cdot \Gamma \cdot (n_T - \delta) \cdot u_{dq}[\delta]\Big) \end{aligned} \tag{10}$$

with

$$\begin{cases} u_{dq}[0] = u_{dq}[k - n_T - 2] \\ u_{dq}[1] = u_{dq}[k - n_T - 1] \\ \vdots \\ u_{dq}[n_T - 1] = u_{dq}[k - 3] \\ u_{dq}[n_T] = u_{dq}[k - 2] \end{cases}; \quad \begin{cases} i_{dq}[0] = i_{dq}[k - n_T] \\ i_{dq}[1] = i_{dq}[k - n_T + 1] \\ \vdots \\ i_{dq}[n_T - 1] = i_{dq}[k - 1] \\ i_{dq}[n_T] = i_{dq}[k] \end{cases}$$

where δ represents the (δ)th sampling point and the $i_{dq}[\delta]$, $u_{dq}[\delta]$ denotes the historical data that sampled during $[t - \Gamma, t]$ time domain and already stored in the database.

By the Eq.(10), the $\hat{X}_{dq}$ can be calculated online by the online data-driven techniques in each sampling period. Moreover, the calculated process of $\hat{X}_{dq}$ is completely independent of the initial system state i_{dq0}, which means the initial value of the historical database could be directly defined as a zero matrix with the same dimension. This feature is different from the existing methods, such as the Kalman Filter, Slide Model Control, Disturbance Observer Control, etc., whose control robustness is quite sensitive to the parameter initialization settings.

To study the stability analysis of the proposed algorithm, the Lyapunov's theory is utilized to verify the convergence of the proposed Model-free method as follows. The Lyapunov function V is presented as [14]

$$V = \frac{1}{2}s^2, s = \hat{i}_{dq} - i_{dq} \tag{11}$$

According to the Lyapunov stability theory, the system is stable when the derivative of the V satisfies Eq.(12).

$$dV/dt = s \cdot (ds/dt) \leq 0 \tag{12}$$

Subtracting Eq.(6) and Eq.(11), the Eq.(12) can be expressed as

$$\begin{aligned} \dot{V} &= s \cdot s' \\ &= s \cdot \left(\frac{d\hat{i}_{dq}}{dt} - \frac{di_{dq}}{dt} \right) = \begin{cases} 0, & s = 0 \\ s \cdot \left(\frac{d\hat{i}_{dq}}{dt} - \frac{di_{dq}}{dt} \right), & s \neq 0 \end{cases} \\ &= \begin{cases} 0, & s = 0 \\ s \cdot \left(\hat{X}'_{dq} + c_{dq} \cdot u_{dq} - X_{dq} - c_{dq} \cdot u_{dq} \right), & s \neq 0 \end{cases} \\ &= \begin{cases} 0, & s = 0 \\ s \cdot \left(\hat{X}'_{dq} - X_{dq} \right), & s \neq 0 \end{cases} \end{aligned} \tag{13}$$

Subtracting (9), the case of "s $\neq$ 0" in Eq.(13) can be expressed as

$$\begin{aligned} \dot{V} &= s \cdot \left(\hat{X}'_{dq} - X_{dq} \right) \\ &= s \cdot \left\{ \frac{3!}{\Gamma^3} \left[(\Gamma - 2\sigma) \cdot i_{dq}(\sigma) + \alpha\sigma (\Gamma - \sigma) \cdot u_{dq}(\sigma) \right] \Big|_0^{\Gamma} - X_{dq} \right\} \\ &= s(k) \cdot \frac{3!}{\Gamma^3} \left[-\Gamma \cdot i_{dq}(k) - \Gamma \cdot i_{dq}(k - \Gamma) - X_{dq}(k) \right] \end{aligned}$$

To ensure the stability of the system, the derivative of the Lyapunov function should be satisfied $\dot{V} \leq 0$, which is

$$\begin{aligned} \dot{V} &= s(k) \cdot \frac{3!}{\Gamma^3} \left[-\Gamma \cdot i_{dq}(k) - \Gamma \cdot i_{dq}(k - \Gamma) - X_{dq}(k) \right] \\ &\leq 0 \Rightarrow \Gamma \geq n_T \cdot T_S = -\frac{s(k) \cdot X_{dq}(k)}{i_{dq}(k) + i_{dq}(k - \Gamma)} \end{aligned} \tag{14}$$

From Eq.(14), the suitable Γ that could achieve the stability of the system can be found.

C. THE ROLLING UPDATE MECHANISM FOR DATA REGISTRATION

To calculate the Eq.(10), the database that includes stator current and voltage measurements sampled in the latest Γ time domain needs to be updated during each sampling period by the rolling update mechanism for data registration, which can be expressed by $u_{dq}[0] \ldots u_{dq}[n_T]$ and $i_{dq}[0] \ldots i_{dq}[n_T]$.

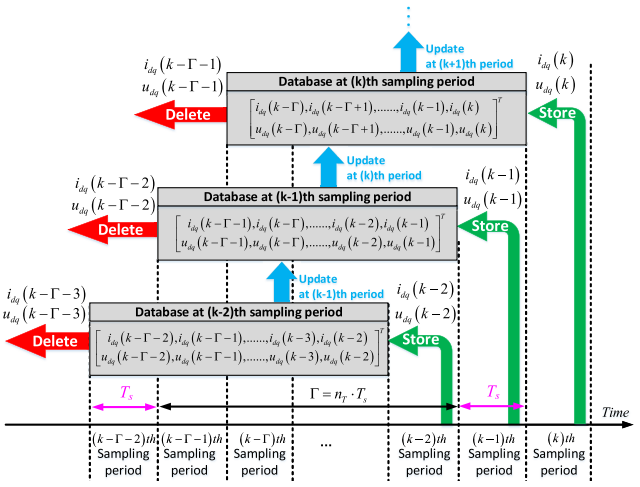

FIGURE 2. The rolling update mechanism of the data storage domain.

The proposed rolling update mechanism of the database is depicted in Fig.2. According to the Fig.2, it can be seen that the database in the microprocessor only registers the stator current/voltage data measured during the latest $\Gamma = n_T \cdot T_s$ time domain. For instance, the database at *(k-1)*th sampling period only registers the stator current/voltage data that were measured from the *(k-Γ-1)*th period to the *(k-1)*th period. Similarly, the database at *(k)*th sampling period only

registers the current/voltage data that were measured from the (k-Γ)th period to the (k)th period.

According to Eq.(10), it can be seen that the estimated accuracy of $\hat{X}_{dq}$ is directly depends on the length of time domain for historical data registration. Considering the limited register space and computing burden of the microprocessor, the stator voltage and current data within the latest n_T sampling periods are updated and registered online. According to Eq.(14), the control stability cannot be guaranteed if the selected time window for historical data registration is too short (while n_T is s too small to satisfy Eq.14). Therefore, based on the simulation and experiment research, only if the optimal length of n_T in the rolling update mechanism satisfies Eq.(15) can ensure the control stability under existing hardware without causing excessive storage requirements and computational burden.

$$n_T = \begin{cases} 11, & i_q^{ref}(k+2) \neq i_q^{ref}(k+1) \\ 15, & i_q^{ref}(k+2) = i_q^{ref}(k+1) \end{cases} \tag{15}$$

Since the weight coefficient of the data in latest sampling periods needs to be increased under dynamic conditions, the data registered in the latest 11 sampling periods are used to calculate the $\hat{X}_{dq}$. On the contrary, to improve the estimated accuracy under steady-state conditions, the data in the latest 15 sampling periods are used in the $\hat{X}_{dq}$ calculation process.

IV. THE MODULATION METHOD BASED ON CURRENT INCREMENT SYNTHESIS

When the PMSM operated under low-speed steady-state working conditions, the negative stator current increment generated by zero-voltage vectors plays a significant role in the current harmonic suppression. However, the modulation algorithm based on reference voltage vector synthesis ignores this feature. Therefore, the predicted current circle tracking modulation, which is based on the stator current increments synthesis, need to be study further [37]. In this paper, a novel modulation method based on current increments synthesis is proposed and described in detail as follows.

Since the character of high sampling frequency in the PMSM drives, the $\hat{X}_{dq}$ calculated at the (k)th period is approximatively equal to the $\hat{X}_{dq}$ at the (k+1)th period under low-speed condition, which can be expressed as $\hat{X}_{dq}(k+1) = \hat{X}_{dq}(k)$. The predicted current $i_{dq}^{pre}(k+1)$ can be obtained by Eq.(7).

$$i_{dq}^{pre}(k+1) = i_{dq}(k) + \left[\hat{X}_{dq}(k) + x_{dq} \cdot u_{dq}(k)\right] \cdot T_s \tag{16}$$

To overcome the stagnant current update mechanism, the eight current increments during the (k+1)th period corresponding to eight-element voltage vectors is designed to update in each sampling period by Eq.(17).

$$\begin{aligned} &\Delta i_{dq}^{pre}(k+1)_w \\ &= \left[\hat{X}_{dq}(k) + x_{dq} \cdot u_{dq}(k+1)_w\right] \cdot T_s; \\ &\qquad w \in \{0, 1, 2, 3, 4, 5, 6, 7\} \end{aligned} \tag{17}$$

$$\begin{aligned} &\Delta i_{dq}^{ref}(k+1) \\ &= i_{dq}^{ref}(k+2) - i_{dq}^{pre}(k+1) \\ &= \begin{bmatrix} \Delta i_d^{ref}(k+1) \\ \Delta i_q^{ref}(k+1) \end{bmatrix} = \begin{bmatrix} i_d^{ref}(k+2) \\ i_q^{ref}(k+2) \end{bmatrix} - \begin{bmatrix} i_d^{pre}(k+1) \\ i_q^{pre}(k+1) \end{bmatrix} \end{aligned} \tag{18}$$

The reference current increment during the (k+1)th sampling period $\Delta i_{dq}^{ref}(k+1)$ can be calculated with reference current at the start of (k+2)th sampling period $i_{dq}^{ref}(k+2)$ and the predicted currents $i_{dq}^{pre}(k+1)$, as shown in Eq.(18).

To eliminate the impact of the rotor position on the calculation accuracy, all kinds of current increments need to be transformed from the *dq-axis* to the *αβ-axis* by inverse Park transformation. The optimal current increment $\Delta i_{\alpha\beta}^{opt}(k+1)$ is selected by the minimization of the cost function as shown in Eq.(19) and defined as the main current increment by Eq.(20).

$$\begin{aligned} J_w = &\left|\Delta i_\alpha^{ref}(k+1) - \Delta i_\alpha^{pre}(k+1)_w\right| \\ &+ \left|\Delta i_\beta^{ref}(k+1) - \Delta i_\beta^{pre}(k+1)_w\right|; \\ &subject\ to\ w \in \{1, 2, 3, 4, 5, 6\}; \end{aligned} \tag{19}$$

$$\begin{aligned} &\Delta i_{\alpha\beta}^{opt}(k+1) = \begin{bmatrix} \Delta i_\alpha^{opt}(k+1) \\ \Delta i_\beta^{opt}(k+1) \end{bmatrix}^T = \begin{bmatrix} \Delta i_\alpha^{pre}(k+1)_j \\ \Delta i_\beta^{pre}(k+1)_j \end{bmatrix}^T \\ &subject\ to\ J_j = \min(J_w); j \in \{1, 2, 3, 4, 5, 6\} \end{aligned} \tag{20}$$

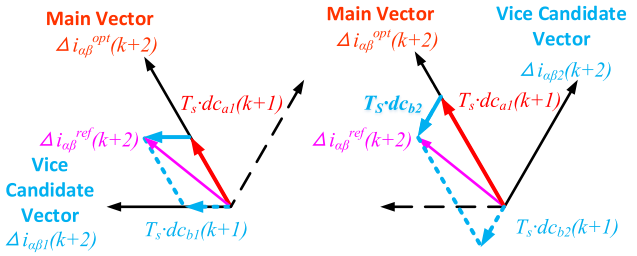

FIGURE 3. The judgment of initial basis current increment duty cycles.

To determine the active vice increment, two active current vectors that adjacent to the main current increment are selected as the vice candidate increments and defined as $(\Delta i_{\alpha 1}, \Delta i_{\beta 1})$ and $(\Delta i_{\alpha 2}, \Delta i_{\beta 2})$. The negative current increments generated by the zero-voltage vectors is defined as another vice current increment $(\Delta i_{\alpha 0}, \Delta i_{\beta 0})$. As a result, there are two sets of basic stator current increments set that could be used for current increments synthesis at (k+1)th sampling period, which are $\left[\left(i_\alpha^{opt}, i_\beta^{opt}\right), (i_{\alpha 1}, i_{\beta 1}), (i_{\alpha 0}, i_{\beta 0})\right]^T$ and $\left[\left(i_\alpha^{opt}, i_\beta^{opt}\right), (i_{\alpha 2}, i_{\beta 2}), (i_{\alpha 0}, i_{\beta 0})\right]^T$. Their corresponding duty cycle are defined as $[dc_{a1}, dc_{b1}, dc_{01}]^T$ and $[dc_{a2}, dc_{b2}, dc_{02}]^T$.

According to the parallelogram rule, the numerical solution of two duty cycle sets can be obtained by solving two sets

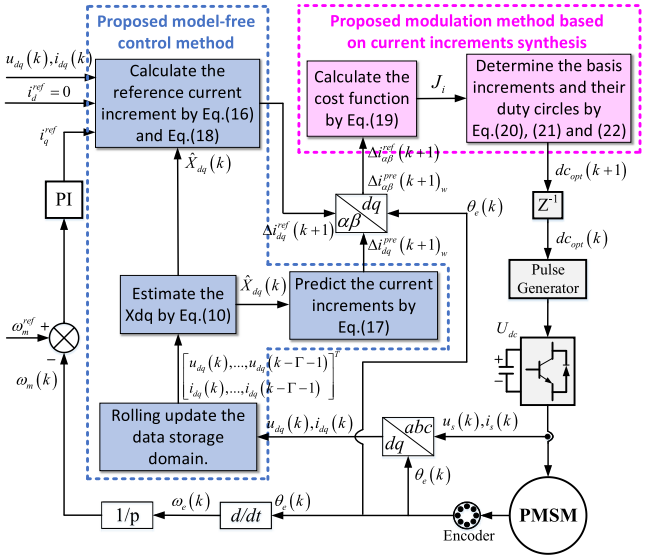

FIGURE 4. The control scheme of the proposed model-free predictive current control method with current increment modulation.

of three-variable linear equations in each period as in (21), shown at the bottom of the page.

However, the numerical solution of the duty cycle is only correct in theory. Any negative solution violates the actual application, as shown in Fig.3. The judgment of the initial duty cycle set at $(k+1)$th sampling period $dc^{ini}(k+1)$ are selected based on Eq.(22).

$$
\begin{aligned}
&dc^{ini}(k+1)\\
&=\begin{bmatrix} dc^{ini}_{main} \\ dc^{ini}_{vice} \\ dc^{ini}_{0} \end{bmatrix}\\
&=\begin{cases}
\begin{bmatrix} dc_{a1}(k+1) \\ dc_{b1}(k+1) \\ dc_{01}(k+1) \end{bmatrix}, (dc_{a1}\geq 0)\cap(dc_{b1}\geq 0)\\
\begin{bmatrix} dc_{a2}(k+1) \\ dc_{b2}(k+1) \\ dc_{02}(k+1) \end{bmatrix}, (dc_{a2}\geq 0)\cap(dc_{b2}\geq 0)
\end{cases}
\end{aligned}
\tag{22}
$$

Moreover, to retain the quick current response of the classic MPCC under dynamic conditions, the $dc^{ini}(k+1)$ needs to be re-corrected by the constraint rules listed in Table 1. Finally, the optimal duty cycle set

TABLE 1. The constraints of the duty cycle.

If	Then
$dc^{ini}_{main}\geq 1;\ 1>dc^{ini}_{vice}\geq 0$	$dc^{opt}_{main}=1;\ dc^{opt}_{vice}=dc^{opt}_{0}=0$
$1>dc^{ini}_{main}\geq 0;\ dc^{ini}_{vice}\geq 1$	$dc^{opt}_{vice}=1;\ dc^{opt}_{main}=dc^{opt}_{0}=0$
$1>dc^{ini}_{main}\geq 0;\ 1>dc^{ini}_{vice}\geq 0;$ $dc^{ini}_{main}+dc^{ini}_{vice}\geq 1$	$dc^{opt}_{main}=dc^{opt}_{main}/(dc^{opt}_{main}+dc^{opt}_{vice});$ $dc^{opt}_{vice}=1-dc^{opt}_{main};\ dc^{opt}_{0}=0$
Except for the above three cases.	$dc^{opt}(k+1)=dc^{ini}(k+1)$

$dc^{opt}(k+1)=\left[dc^{opt}_{main}, dc^{opt}_{vice}, dc^{opt}_{0}\right]^T$ is obtained and delivered to the 2-Level voltage sources inverter (2L-VSI) by pulse generator. The 5-segment conducted method is utilized and the switch state of the negative current increment is always set to (000) in this paper. The control strategy scheme of the proposed model-free control algorithm is shown in Fig.4.

V. EXPERIMENTAL VERIFICATION

A. EXPERIMENT BENCH CALIBRATION

To evaluate the effectiveness of the proposed model-free predictive current control algorithm, a certain type of SPMSM is chosen as the control target and its rated parameters are listed in Table 2. Since the method proposed in this paper is aimed to deploy under low-speed conditions, the "$i^{ref}_d=0$" control method is applied in the experiment. The experimental platform is established as shown in Fig.5. The SPMSM is driven by a 2-level voltage source inverter (2L-VSI) with Fairchild FNC42060F semiconductor power modules. The TMS320F28377D microprocessor is used to deploy the proposed model-free control method and carry out the pulse-generated operation. The sampling frequency in the experiment is set to 20kHz.

The classical MPCC, the nonparametric predictive current control (NPCC) method with reference voltage vector synthesis modulation in [36], and the improved model-free predictive current control (IMFPCC) proposed in this paper are conducted in the experimental verification. The typical current step operations with different speeds and load torque are executed in the experimental verification.

B. RESULT ANALYZED

The experimental results of the *dq-axis* stator current by three control algorithms under the rated motor parameters at 800r/min are shown in Fig.6. The load torque is set as 2-6-4Nm. Due to the larger modulated error in theory, the

$$
\begin{cases}
\begin{bmatrix} \Delta i^{opt}_{\alpha}(k+1) & \Delta i_{\alpha 1}(k+1) & \Delta i_{\alpha 0}(k+1) \\ \Delta i^{opt}_{\beta}(k+1) & \Delta i_{\beta 1}(k+2) & \Delta i_{\beta 0}(k+1) \\ 1 & 1 & 1 \end{bmatrix}\cdot\begin{bmatrix} dc_{a1}(k+1) \\ dc_{b1}(k+1) \\ dc_{01}(k+1) \end{bmatrix}=\begin{bmatrix} \Delta i^{ref}_{\alpha}(k+1) \\ \Delta i^{ref}_{\beta}(k+1) \\ 1 \end{bmatrix}\\
\begin{bmatrix} \Delta i^{opt}_{\alpha}(k+1) & \Delta i_{\alpha 2}(k+1) & \Delta i_{\alpha 0}(k+1) \\ \Delta i^{opt}_{\beta}(k+1) & \Delta i_{\beta 2}(k+1) & \Delta i_{\beta 0}(k+1) \\ 1 & 1 & 1 \end{bmatrix}\cdot\begin{bmatrix} dc_{a2}(k+1) \\ dc_{b2}(k+1) \\ dc_{02}(k+1) \end{bmatrix}=\begin{bmatrix} \Delta i^{ref}_{\alpha}(k+1) \\ \Delta i^{ref}_{\beta}(k+1) \\ 1 \end{bmatrix}
\end{cases}
\tag{21}
$$

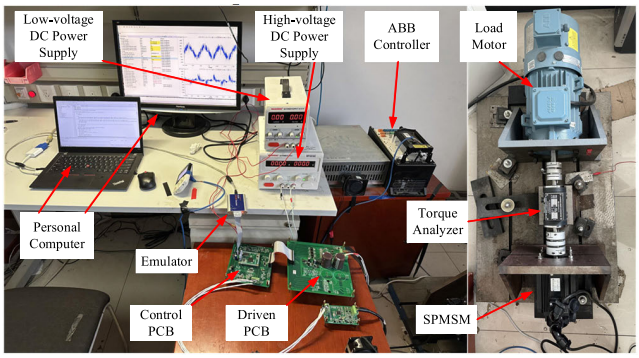

FIGURE 5. The test equipment platform of SPMSM drive system.

TABLE 2. The SPMSM's rated parameters.

Parameter	Value	Parameter	Value
Rated speed ω_m(r/min)	1000	Rated stator resistance $R_s'(\Omega)$	0.365
Max torque T_N(Nm)	10	Rated stator inductance L_s'(mH)	1.225
Max current I_N(A)	10	Rated rotor flux linkage Ψ_r'(Wb)	0.1667
Pole pairs number p	4	DC-Bus voltage U_{DC}(V)	130

single voltage vector modulation of MPCC causes huge current harmonics. Benefiting from the current increments synthesis modulation that includes the negative current increment, the IMFPCC could suppress the current harmonic more effectively than the NPCC.

Fig.7 shows the experiment results of the *dq-axis* current under $R_s = 0.1R_s'$ at 600r/min and 3-6-4Nm load torque. Compared with Fig.6, the current control performance of the three methods in Fig.7 does not deteriorate significantly with the stator resistance decreasing.

Fig.8 demonstrates the experiment results of the *dq-axis* current under $R_s = 10R_s'$ at 600r/min and 2-9-5Nm load torque. With the stator resistance increasing, there is a positively *q-axis* current tracking offset that is positively proportional to the load torque in Fig.8(a). According to Fig.8(b) and Fig.8(c), the NPCC and IMFPCC both have the ability to detect the variation of R_s and eliminate the i_q tracking offset. However, the IMFPCC provides a better current harmonic suppression performance. At the instant of load-torque reduce from 9Nm to 5Nm, there is a tiny current overshoot in Fig.8(c) and an identified offset of $\hat{X}_q$ also appears in Fig.8(e). The reason is that the n_T is switched from 15 to 11 and the single current increment conduction is applied under dynamic condition. Then, the calculation of $\hat{X}_{dq}$ converges to its actual value with the n_T is set to 15 again.

The experiment results under $\Psi_r = 0.5\Psi_r'$ mismatching at 800r/min are shown in Fig.9. The load torque is set as 3-8-2Nm. Due to the decreasing of the rotor flux linkage Ψ_r, there is a "-2A" negative tracking offset between the $i_q(k)$ and the $i_q^{ref}(k)$ under MPCC control in Fig.9(a). Comparing to the NPCC in Fig.9(b), the IMFPCC eliminates the $i_q(k)$ tracking offset with the smallest current harmonics, as shown in Fig.9(c). However, there is a overshoot *q-axis* current at the instant of load torque step-down response in Fig.9(c). And then, the calculated $\hat{X}_{dq}$ converges to its actual value when the data of the new steady-state condition are updated in the database, as shown in Fig.9(e).

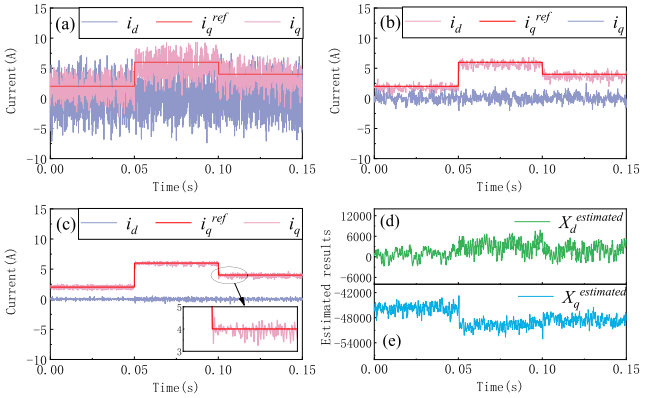

FIGURE 6. Experimental results with rated motor parameters at 800r/min and 2-6-4Nm. (a)MPCC; (b)NPCC; (c)IMFPCC; (d)(e)Estimated results of X_{dq}.

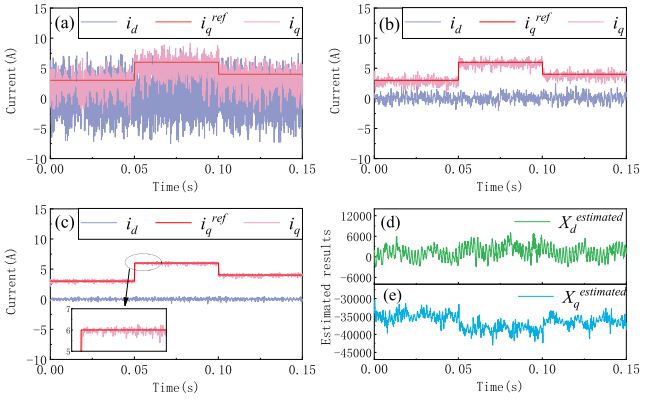

FIGURE 7. Experimental results under $R_s = 0.1R_s'$ mismatching at 600r/min and 3-6-4Nm. (a)MPCC; (b)NPCC; (c)IMFPCC; (d)(e)Estimated results of X_{dq}.

On the opposite, the experiment results of the *dq-axis* current under $\Psi_r = 2\Psi_r'$ at 800r/min and 2-6-4Nm load torque are shown in Fig.10. Due to the increasing of the Ψ_r, there is about a "+4A" positive tracking offset between the $i_q(k)$ and the $i_q^{ref}(k)$ by MPCC in Fig.10(a). And, there is still a tiny negative offset in i_q^{ref} tracking by NPCC, as shown in Fig.10(b). The IMFPCC eliminates the $i_q(k)$ tracking offset with smallest current harmonics, as shown in Fig.10(c).

Fig.11 shows the experiment results under $L_s = 0.5L_s'$ at 400r/min. The load torque is set as 4-8-2Nm. With the speed decreasing to 400r/min, there are huge *dq-axis* stator current harmonics under MPCC control, as shown in Fig.11(a). In Fig.11(c), there is a 50% overshoot in i_q tracking control and distorted $\hat{X}_{dq}$ estimation results at the instant of "8-2Nm" step-down condition. However, within about 0.002 seconds, the i_q convergences to the i_q^{ref} and the $\hat{X}_{dq}$ convergences to its actual value. Compared with the stator resistance and rotor flux variation, the stator inductance mismatching causes

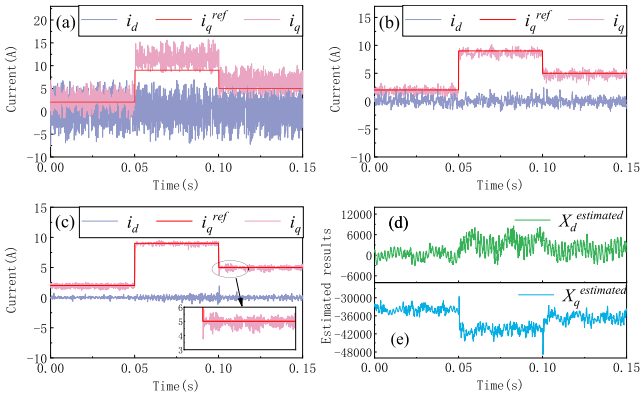

FIGURE 8. Experimental results under $R_S = 10R_S'$ mismatching at 600r/min and 2-9-5Nm. (a)MPCC; (b)NPCC; (c)IMFPCC; (d)(e)Estimated results of X_{dq}.

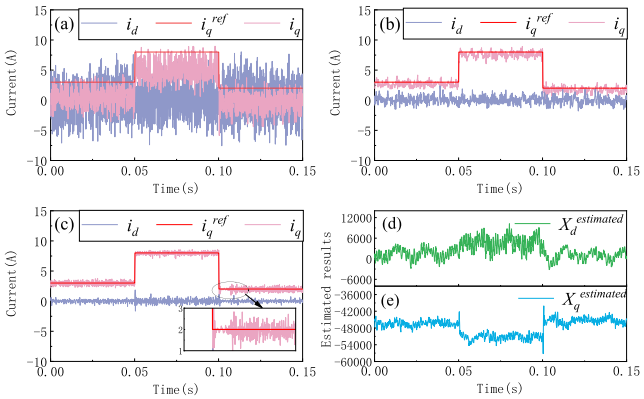

FIGURE 9. Experimental results under $\Psi_r = 0.5\Psi_r'$ mismatching at 800r/min and 3-8-2Nm. (a)MPCC; (b)NPCC; (c)IMFPCC; (d)(e)Estimated results of X_{dq}.

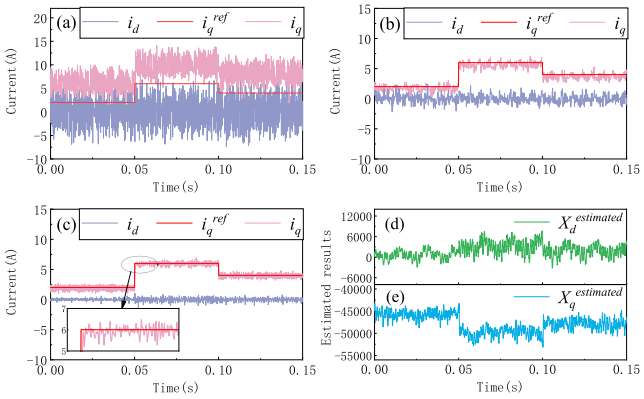

FIGURE 10. Experimental results under $\Psi_r = 2\Psi_r'$ mismatching at 800r/min and 2-6-4Nm. (a)MPCC; (b)NPCC; (c)IMFPCC; (d)(e)Estimated results of X_{dq}.

significant fluctuation in the estimated results of $\hat{X}_\mathrm{d}$, even when the system is operating under steady-state conditions, as shown in Fig.11(d). The reason for this phenomenon is that the value of L_s occupies a larger numerical weight than the R_s and Ψ_r does in the stator current prediction mathematical model that expressed as Eq.(5). Benefit from the proposed rolling data update mechanism, the $\hat{X}_\mathrm{d}$ calculated result converges to its real value with acceptable vibration amplitude.

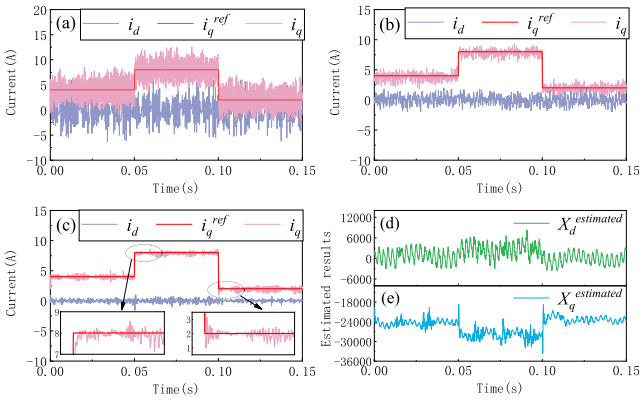

FIGURE 11. Experimental results under $L_S = 0.5L_S'$ mismatching at 400r/min and 4-8-2Nm. (a)MPCC; (b)NPCC; (c)IMFPCC; (d)(e)Estimated results of X_{dq}.

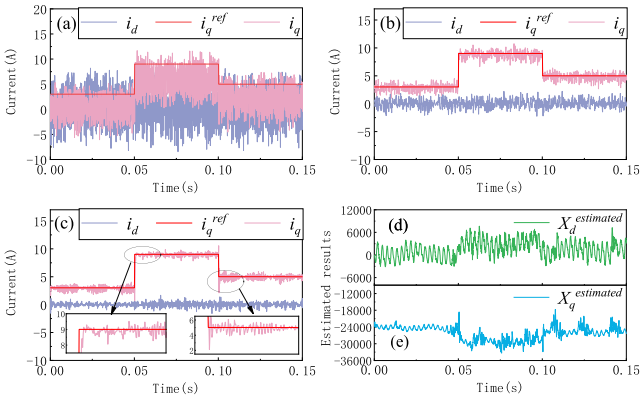

FIGURE 12. Experimental results under $L_S = 2L_S'$ mismatching at 400r/min and 3-9-5Nm. (a)MPCC; (b)NPCC; (c)IMFPCC; (d)(e)Estimated results of X_{dq}.

Fig.12 shows the experiment results of stator current under $L_s = 2L_s'$ at 400r/min and 3-9-5Nm load torque. When the L_s becomes larger and the rotator's speed reduces to 400r/min, the MPCC method leads to a negative deviation of -3A in q-axis current tracking with huge current harmonics, as shown in Fig.12 (a). Since the stator inductance increasing, the single current increment modulation in IMPCC produces outstanding current overshoots at the instant of current step operations, as shown in Fig.12(c). However, this corresponding feature cannot be found under NPCC control, as shown in Fig.12(b).

Fig.13 shows the experimental results of the *dq-axis* current under $R_s = 0.5R_s'$, $\Psi_r = 1.5\Psi_r'$, $L_s = 0.5L_s'$ at 500r/min. The load torque is set as 2-7-5Nm. Under the mismatching of R_s, L_s and Ψ_r, there is a positive deviation of +3A between the $i_q(k)$ and the $i_q^{ref}(k)$ in Fig.13(a). According to the Fig.13(c) and (d), it can be seen that IMFPCC causes a 30% overshoot current at the instant of load torque decreases from

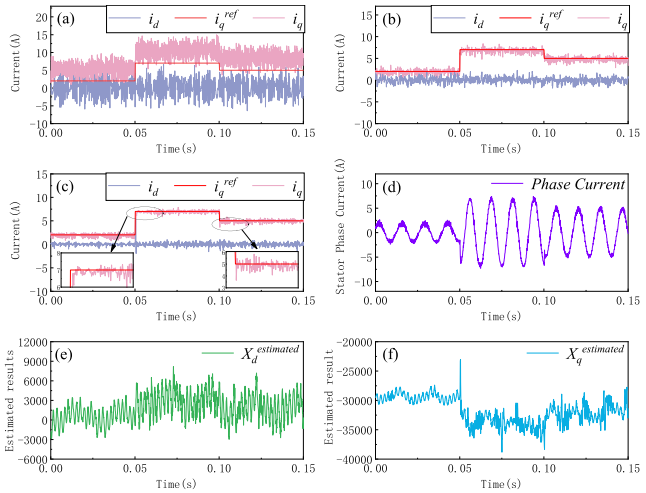

FIGURE 13. Experimental results under $R_s = 0.5R_s'$, $\Psi_r = 1.5\Psi_r'$, $L_s = 0.5L_s'$ mismatching at 500r/min and 2-7-5Nm. (a)MPCC; (b)NPCC; (c)IMFPCC; (d)Phase current under IMFPCC;(e)(f)Estimated results of X_{dq}.

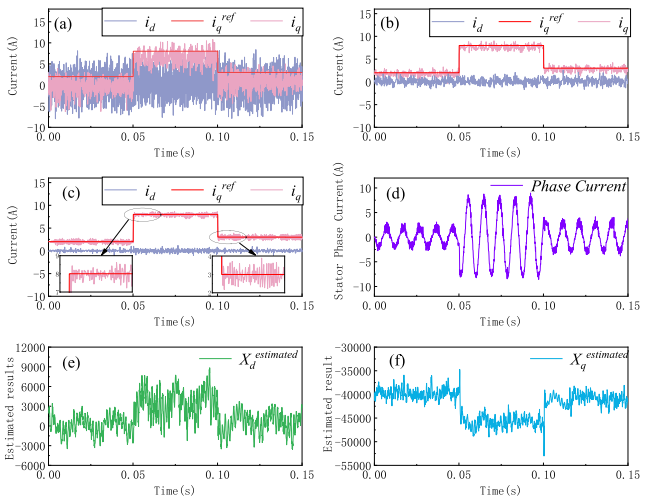

FIGURE 14. Experimental results under $R_s = 10R_s'$, $\Psi_r = 0.5\Psi_r'$, $L_s = 1.5L_s'$ mismatching at 700r/min and 2-8-3Nm. (a)MPCC; (b)NPCC; (c)IMFPCC; (d)Phase current under IMFPCC;(e)(f)Estimated results of X_{dq}.

7Nm to 5Nm. In Fig.13(e), the $\hat{X}_\mathrm{d}$ still vibrated around its actual value caused by mismatched inductance.

Similarly, the Fig. 14 shows the experimental results of the *dq-axis* current under $R_s = 10R_s'$, $\Psi_r = 0.5\Psi_r'$, $L_s = 1.5L_s'$ at 700r/min. The load torque is set as 2-8-3Nm. There is a negative deviation of -2A between the $i_q\,(k)$ and the $i_q^{ref}\,(k)$ by MPCC in Fig.14(a). Benefiting from the proposed current increments synthesis modulation, the IMFPCC provides better stator current harmonic suppression performance than the NPCC when the system operates at 700r/min, as shown in Fig.14(b) and (c). Since the multi-parameters mismatching, there are overshoot results in the $\hat{X}_q$ calculation under dynamic conditions, as shown in Fig14(f).

Fig.15 shows the experimental results of the *dq*-axis current under $R_s = 0.5R_s'$, $\Psi_r = 1.5\Psi_r'$, $L_s = 0.5L_s'$ at 100r/min.

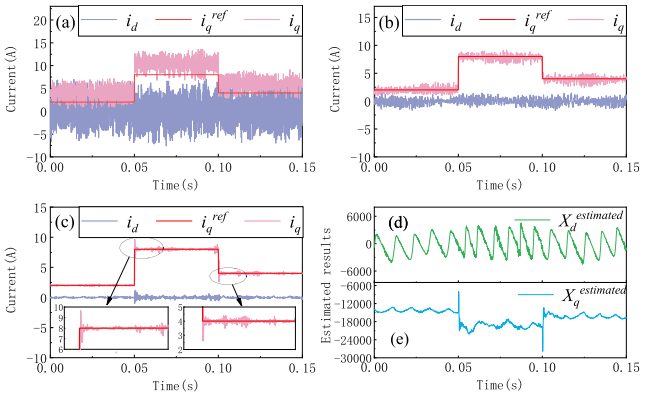

FIGURE 15. Experimental results under $R_s = 0.5R_s'$, $\Psi_r = 1.5\Psi_r'$, $L_s = 0.5L_s'$ mismatching at 100r/min and 2-8-4Nm. (a)MPCC; (b)NPCC; (c)IMFPCC;(d)(e)Estimated results of X_{dq}.

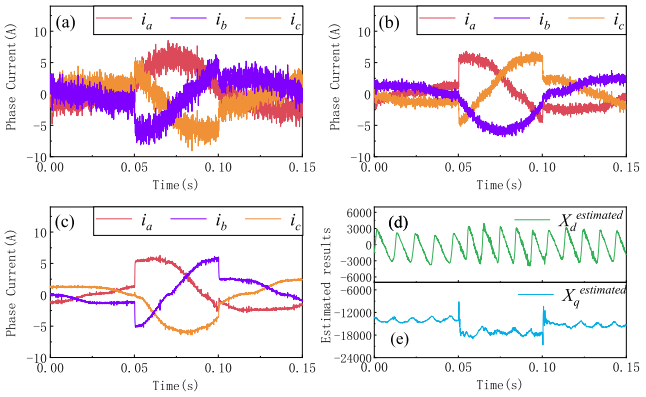

FIGURE 16. Experimental results under $R_s = 10R_s'$, $\Psi_r = 0.5\Psi_r'$, $L_s = 1.5L_s'$ mismatching at 50r/min and 2-6-3Nm. (a)MPCC; (b)NPCC; (c)IMFPCC;(d)(e)Estimated results of X_{dq}.

Due to the increasing of Ψ_r, the positive deviation between $i_q\,(k)$ and $i_q^{ref}\,(k)$ still existed in Fig.15(a). Comparing with the Fig.15 (b), the IMFPCC provides better current harmonics suppression under steady-state condition, but it still produces large overshoot under the dynamcs condition, as shown in Fig.15 (c).

Fig.16 shows the experimental results of the stator phase current under $R_s = 10R_s'$, $\Psi_r = 0.5\Psi_r'$, $L_s = 1.5L_s'$ at 50r/min. Fig.16(a) shows that the current harmonics become larger under MPCC control when the rotor speed decreases to 50r/min. Comparing the (b) and (c) in Fig.16, it can be seen that the modulation based on current increments synthesis could improve the effect of negative current increment in the current harmonics suppression, especially under the low-speed conditions.

Fig.17 shows the experimental results of the dq-axis current under $R_s = 10R_s'$, $\Psi_r = 0.5\Psi_r'$, $L_s = 1.5L_s'$ from 0 to 1000r/min without load-torque. The MPCC produces large current harmonics and longer response time as shown in Fig.17 (a) and (b). The NPCC could achieve the 1000r/min within a shorter response time than the MPCC dose as shown in Fig.17 (c) and (d). The IMFPCC provides

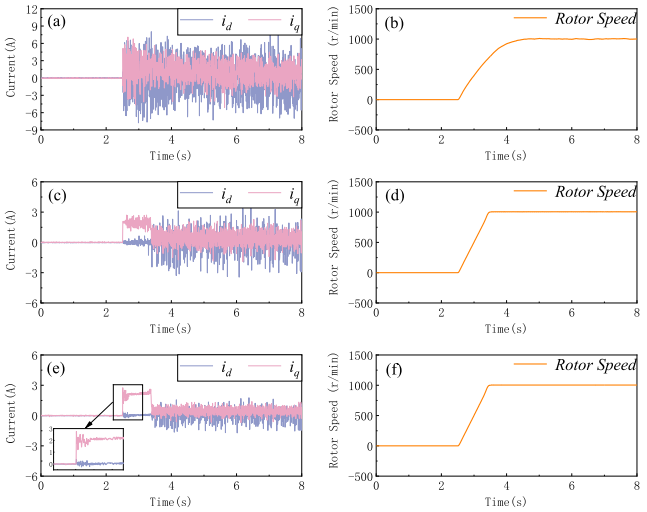

FIGURE 17. Experimental results under $R_s = 10R_s'$, $\Psi_r = 0.5\Psi_r'$, $L_s = 1.5L_s'$ mismatching from 0 to 1000r/min without load torque. (a),(b)MPCC; (c),(d)NPCC; (e),(f)IMFPCC.

the best current harmonics suppression during the whole process as shown in Fig.17 (e) and (f). However, there is current oscillation at the beginning of the start-up condition caused by the inappropriate $\hat{X}_{dq}$ calculated by the zero-initialized data in the rolling update mechanism database. Benefitting from the high frequency of the control algorithm and the data rolling update mechanism, the $\hat{X}_{dq}$ converges to its actual value in a short time.

To compare the stator current control performance of three methods in the experiments mentioned above, two tracking assessment criteria of *q-axis* current i_q are set as Eq.(23). The calculated results of three methods are listed in Table 3 and Table 4. Moreover, the Total Harmonic Distortion (THD) of the three control methods in Fig.13 and Fig.14 are also listed in Table 5.

$$\begin{cases} M_i = \dfrac{1}{N}\displaystyle\sum_{k=1}^{N}\left|i_q^{ref}(k) - i_q(k)\right| \\ J_i = \sqrt{\dfrac{1}{N}\displaystyle\sum_{k=1}^{N}\left(i_q^{ref}(k) - i_q(k)\right)^2} \end{cases} \tag{23}$$

where N denotes the total number of sampling points.

To compare the instantaneous computational burden of the three control methods, the step calculation function provided by the Code Composer Studio 8.2.0 software is utilized to count the computational time while the algorithm runs from the start line to the end line within a single sampling period. The computation time of each method are listed in Table 6. The proposed IMFPCC costs the longest computational time than the other methods, which is caused by the updating of the data registration domain and the execution of the proposed model-free control algorithm.

However, according to the results in Table 3 to Table 5, it can be seen that the proposed IMFPCC eliminates the model dependency of MPCC effectively and provides better current harmonics suppression performance than the other two methods.

TABLE 3. Comparison of M_i under the conditions mentioned above.

Operation	MPCC	NPCC	IMFPCC
800r/min, 2-6-4Nm under rated parameters	1.398	0.426	0.179
600r/min, 3-6-4Nm under $R_s = 0.1R_s'$	1.535	0.463	0.138
600r/min, 2-9-5Nm under $R_s = 10R_s'$	1.951	0.447	0.209
800r/min, 3-8-2Nm under $\Psi_r = 0.5\Psi_r'$	2.707	0.448	0.243
800r/min, 2-6-4Nm under $\Psi_r = 2\Psi_r'$	3.961	0.451	0.257
400r/min, 4-8-2Nm under $L_s = 0.5L_s'$	1.667	0.481	0.203
400r/min, 3-9-5Nm under $L_s = 2L_s'$	3.141	0.503	0.298
500r/min, 2-7-5Nm under $R_s = 0.5R_s'$, $\Psi_r = 1.5\Psi_r', L_s = 0.5L_s'$	3.404	0.442	0.261
700r/min, 2-8-3Nm under $R_s = 10R_s'$, $\Psi_r = 0.5\Psi_r', L_s = 1.5L_s'$	2.213	0.438	0.296

TABLE 4. Comparison of J_i under the conditions mentioned above.

Operation	MPCC	NPCC	IMFPCC
800r/min, 2-6-4Nm under rated parameters	1.727	0.539	0.237
600r/min, 3-6-4Nm under $R_s = 0.1R_s'$	1.974	0.582	0.192
600r/min, 2-9-5Nm under $R_s = 10R_s'$	2.403	0.569	0.342
800r/min, 3-8-2Nm under $\Psi_r = 0.5\Psi_r'$	3.083	0.561	0.343
800r/min, 2-6-4Nm under $\Psi_r = 2\Psi_r'$	4.323	0.565	0.341
400r/min, 4-8-2Nm under $L_s = 0.5L_s'$	1.992	0.609	0.344
400r/min, 3-9-5Nm under $L_s = 2L_s'$	3.839	0.643	0.531
500r/min, 2-7-5Nm under $R_s = 0.5R_s'$, $\Psi_r = 1.5\Psi_r', L_s = 0.5L_s'$	3.882	0.563	0.457
700r/min, 2-8-3Nm under $R_s = 10R_s'$, $\Psi_r = 0.5\Psi_r', L_s = 1.5L_s'$	2.687	0.557	0.412

TABLE 5. THD(%) comparison of three control methods.

Operation	Load torque	MPCC	NPCC	IMFPCC
500r/min under $R_s = 0.5R_s'$, $\Psi_r = 1.5\Psi_r'$, $L_s = 0.5L_s'$ in Fig.13	2Nm	110.374%	34.873%	20.438%
	7Nm	45.292%	15.251%	9.674%
	5Nm	68.073%	22.632%	14.961%
700r/min under $R_s = 10R_s'$, $\Psi_r = 0.5\Psi_r'$, $L_s = 1.5L_s'$ in Fig.14	2Nm	94.625%	26.911%	17.102%
	8Nm	40.435%	12.407%	8.351%
	3Nm	92.863%	25.634%	16.673%

TABLE 6. Computation time of three control methods.

	MPCC	NPCC	IMFPCC
Computation Time	17.12 μs	22.68μs	28.27 μs

VI. CONCLUSION

To overcome the model dependency and current harmonic under low-speed steady-state conditions of MPCC, an improved model-free predictive current control method with stator current increment synthesis modulation is proposed in this paper. The achievements and the innovation of it can be summarized as follows.

1) An improved model-free predictive current control method based on data-driven is proposed to get rid of the

parameter dependency of stator current predicted model in MPCC under low-speed conditions, and avoid the deterioration of stator current prediction accuracy caused by motor parameters mismatching effectively. By this method, the unknown polynomial in the stator current predicted model that related to all SPMSM parameters can be estimated simultaneously as the lumped term;

2) A rolling online data update mechanism with variable-time window is proposed to ensure the estimated accuracy of the unknown lumped term with lower computational burden and less RAM space requirement. Moreover, the initial data in the proposed rolling update mechanism database can be set as a zero matrix directly, which is different from the existing control methods whose predicted accuracy is sensitive to the parameter initialization settings;

3) A novel modulation method based on the reference stator current increment synthesis is proposed to reduce current harmonic by solving the conducted time of the corresponding switching state from the stator current increment linear equations. By this method, the negative current increment generated by the zero-voltage vector can be used to suppress current harmonic effectively under low-speed steady-state conditions, and the quick current response of MPCC under dynamic conditions can be retained by the proposed constraints of duty cycle.

Even though the proposed model-free control algorithm and modulation method have the advantages mentioned above, there are still some limitations that need to be declared. The proposed modulation method is designed to operate under low-speed steady-state conditions. With the rotator speed increasing, the superiority of the proposed modulation method in current harmonics suppression might disappear. Moreover, the changing process of motor parameters could divided into two types in the actual operation, which include ''gradual change'' and ''sudden change''. Since its high sampling frequency, the motor control algorithm could detect the motor parameter mismatching and treat them as ''gradual change'' in theory. However, due to limited hardware facilities, this paper did not have the ability to conduct the experimental verification for the effectiveness of the proposed method under different parameter changing types.

The defects of proposed algorithm mentioned above needs to study further in the future.

REFERENCES

[1] J. Chen, Y. Qin, A. M. Bozorgi, and M. Farasat, ''Low complexity dual-vector model predictive current control for surface-mounted permanent magnet synchronous motor drives,'' *IEEE J. Emerg. Sel. Topics Power Electron.*, vol. 8, no. 3, pp. 2655–2663, Sep. 2020.
[2] S. Bolognani, S. Calligaro, and R. Petrella, ''Adaptive flux-weakening controller for interior permanent magnet synchronous motor drives,'' *IEEE J. Emerg. Sel. Topics Power Electron.*, vol. 2, no. 2, pp. 236–248, Jun. 2014.
[3] Z. Han and J. Liu, ''Comparative analysis of vibration and noise in IPMSM considering the effect of MTPA control algorithms for electric vehicles,'' *IEEE Trans. Power Electron.*, vol. 36, no. 6, pp. 6850–6862, Jun. 2021.
[4] S. Bolognani, S. Bolognani, L. Peretti, and M. Zigliotto, ''Design and implementation of model predictive control for electrical motor drives,'' *IEEE Trans. Ind. Electron.*, vol. 56, no. 6, pp. 1925–1936, Jun. 2009.
[5] X. Li, W. Tian, X. Gao, Q. Yang, and R. Kennel, ''A generalized observer-based robust predictive current control strategy for PMSM drive system,'' *IEEE Trans. Ind. Electron.*, vol. 69, no. 2, pp. 1322–1332, Feb. 2022.
[6] P. Cortes, M. P. Kazmierkowski, R. M. Kennel, D. E. Quevedo, and J. Rodriguez, ''Predictive control in power electronics and drives,'' *IEEE Trans. Ind. Electron.*, vol. 55, no. 12, pp. 4312–4324, Dec. 2008.
[7] J. Yang, W.-H. Chen, S. Li, L. Guo, and Y. Yan, ''Disturbance/uncertainty estimation and attenuation techniques in PMSM drives—A survey,'' *IEEE Trans. Ind. Electron.*, vol. 64, no. 4, pp. 3273–3285, Apr. 2017.
[8] N. Hamouda, B. Babes, S. Kahla, and Y. Soufi, ''Real time implementation of grid connected wind energy systems: Predictive current controller,'' in *Proc. 1st Int. Conf. Sustain. Renew. Energy Syst. Appl. (ICSRESA)*, Dec. 2019, pp. 1–6.
[9] A. Bouafassa, L. Rahmani, B. Babes, and R. Bayindir, ''Experimental design of a finite state model predictive control for improving power factor of boost rectifier,'' in *Proc. IEEE 15th Int. Conf. Environ. Electr. Eng. (EEEIC)*, Jun. 2015, pp. 1556–1561.
[10] B. Babes, N. Hamouda, S. Kahla, H. Amar, and S. S. M. Ghoneim, ''Fuzzy model based multivariable predictive control design for rapid and efficient speed-sensorless maximum power extraction of renewable wind generators,'' *Electr. Eng. Electromechanics*, no. 3, pp. 51–62, May 2022.
[11] B. Talbi, F. Krim, A. Laib, A. Sahli, and B. Babes, ''A sugeno-fuzzy tuning approach of weighting factor in model predictive control for PV grid-tied PUC7 multi-level inverter,'' in *Proc. 3rd Int. Conf. Smart Grid Renew. Energy (SGRE)*, Mar. 2022, pp. 1–6.
[12] F. Toso, D. Da Rù, P. Alotto, and S. Bolognani, ''A moving horizon estimator for the speed and rotor position of a sensorless PMSM drive,'' *IEEE Trans. Power Electron.*, vol. 34, no. 1, pp. 580–587, Jan. 2019.
[13] Z. Yin, G. Li, Y. Zhang, J. Liu, X. Sun, and Y. Zhong, ''A speed and flux observer of induction motor based on extended Kalman filter and Markov chain,'' *IEEE Trans. Power Electron.*, vol. 32, no. 9, pp. 7096–7117, Sep. 2017.
[14] Y. Zhou, S. Zhang, C. Zhang, X. Li, X. Li, and X. Yuan, ''Current prediction error based parameter identification method for SPMSM with deadbeat predictive current control,'' *IEEE Trans. Energy Convers.*, vol. 36, no. 3, pp. 1700–1710, Sep. 2021.
[15] M. Boussak, ''Implementation and experimental investigation of sensorless speed control with initial rotor position estimation for interior permanent magnet synchronous motor drive,'' *IEEE Trans. Power Electron.*, vol. 20, no. 6, pp. 1413–1422, Nov. 2005.
[16] Z. Chen, M. Tomita, S. Doki, and S. Okuma, ''An extended electromotive force model for sensorless control of interior permanent-magnet synchronous motors,'' *IEEE Trans. Ind. Electron.*, vol. 50, no. 2, pp. 288–295, Apr. 2003.
[17] Y. A-R. I. Mohamed, ''Design and implementation of a robust current-control scheme for a PMSM vector drive with a simple adaptive disturbance observer,'' *IEEE Trans. Ind. Electron.*, vol. 54, no. 4, pp. 1981–1988, Aug. 2007.
[18] H. Liu and S. Li, ''Speed control for PMSM servo system using predictive functional control and extended state observer,'' *IEEE Trans. Ind. Electron.*, vol. 59, no. 2, pp. 1171–1183, Feb. 2012.
[19] J. Qu, C. Zhang, J. Jatskevich, and S. Zhang, ''Deadbeat harmonic current control of permanent magnet synchronous machine drives for torque ripple reduction,'' *IEEE J. Emerg. Sel. Topics Power Electron.*, vol. 10, no. 3, pp. 3357–3370, Jun. 2022.
[20] L. Qu, W. Qiao, and L. Qu, ''An extended-state-observer-based sliding-mode speed control for permanent-magnet synchronous motors,'' *IEEE J. Emerg. Sel. Topics Power Electron.*, vol. 9, no. 2, pp. 1605–1613, Apr. 2021.
[21] Y. Zhang, J. Jin, and L. Huang, ''Model-free predictive current control of PMSM drives based on extended state observer using ultralocal model,'' *IEEE Trans. Ind. Electron.*, vol. 68, no. 2, pp. 993–1003, Feb. 2021.
[22] X. Zhang, Y. Cheng, Z. Zhao, and Y. He, ''Robust model predictive direct speed control for SPMSM drives based on full parameter disturbances and load observer,'' *IEEE Trans. Power Electron.*, vol. 35, no. 8, pp. 8361–8373, Aug. 2020.
[23] Y. Han, C. Gong, L. Yan, H. Wen, Y. Wang, and K. Shen, ''Multiobjective finite control set model predictive control using novel delay compensation technique for PMSM,'' *IEEE Trans. Power Electron.*, vol. 35, no. 10, pp. 11193–11204, Oct. 2020.
[24] J. Wang, Y. Liu, J. Yang, F. Wang, and J. Rodríguez, ''Adaptive integral extended state observer-based improved multistep FCS-MPCC for PMSM,'' *IEEE Trans. Power Electron.*, vol. 38, no. 9, pp. 11260–11276, Sep. 2023.
[25] M. Fliess and C. Join, ''Model-free control,'' *Int. J. Control*, vol. 86, no. 12, pp. 2228–2252, 2013.

[26] J.-W. Jung, V. Q. Leu, T. D. Do, E.-K. Kim, and H. H. Choi, "Adaptive PID speed control design for permanent magnet synchronous motor drives," *IEEE Trans. Power Electron.*, vol. 30, no. 2, pp. 900–908, Feb. 2015.
[27] M. Tursini, F. Parasiliti, and D. Zhang, "Real-time gain tuning of PI controllers for high-performance PMSM drives," *IEEE Trans. Ind. Appl.*, vol. 38, no. 4, pp. 1018–1026, Aug. 2002.
[28] J. G. Cintron-Rivera, S. N. Foster, C. A. Nino-Baron, and E. G. Strangas, "High performance controllers for interior permanent magnet synchronous machines using look-up tables and curve-fitting methods," in *Proc. Int. Electr. Mach. Drives Conf.*, May 2013, pp. 268–275.
[29] J. Lara, J. Xu, and A. Chandra, "A novel algorithm based on polynomial approximations for an efficient error compensation of magnetic analog encoders in PMSMs for EVs," *IEEE Trans. Ind. Electron.*, vol. 63, no. 6, pp. 3377–3388, Jun. 2016.
[30] X. Zhang, C. Zhang, Z. Wang, and J. Rodríguez, "Motor-parameter-free model predictive current control for PMSM drives," *IEEE Trans. Ind. Electron.*, vol. 71, no. 6, pp. 5443–5452, Jun. 2024.
[31] A. Brosch, S. Hanke, O. Wallscheid, and J. Böcker, "Data-driven recursive least squares estimation for model predictive current control of permanent magnet synchronous motors," *IEEE Trans. Power Electron.*, vol. 36, no. 2, pp. 2179–2190, Feb. 2021.
[32] C. Ma, H. Li, X. Yao, Z. Zhang, and F. De Belie, "An improved model-free predictive current control with advanced current gradient updating mechanism," *IEEE Trans. Ind. Electron.*, vol. 68, no. 12, pp. 11968–11979, Dec. 2021.
[33] F. Yu, C. Zhou, X. Liu, and C. Zhu, "Model-free predictive current control for three-level inverter-fed IPMSM with an improved current difference updating technique," *IEEE Trans. Energy Convers.*, vol. 36, no. 4, pp. 3334–3343, Dec. 2021.
[34] X. Yuan, S. Zhang, and C. Zhang, "Nonparametric predictive current control for PMSM," *IEEE Trans. Power Electron.*, vol. 35, no. 9, pp. 9332–9341, Sep. 2020.
[35] J. Wang, H. Yang, Y. Liu, and J. Rodríguez, "Low-cost multistep FCS-MPCC for PMSM drives using a DC link single current sensor," *IEEE Trans. Power Electron.*, vol. 37, no. 9, pp. 11034–11044, Sep. 2022.
[36] Y. Zhou, H. Li, R. Liu, and J. Mao, "Continuous voltage vector model-free predictive current control of surface mounted permanent magnet synchronous motor," *IEEE Trans. Energy Convers.*, vol. 34, no. 2, pp. 899–908, Jun. 2019.
[37] X. Sun, M. Wu, G. Lei, Y. Guo, and J. Zhu, "An improved model predictive current control for PMSM drives based on current track circle," *IEEE Trans. Ind. Electron.*, vol. 68, no. 5, pp. 3782–3793, May 2021.
[38] M. Fliess and H. Sira-Ramírez, "Closed-loop parametric identification for continuous-time linear systems via new algebraic techniques," in *Identification of Continuous-time Models From Sampled Data* (Advances in Industrial Control). London, U.K.: Springer, 2008, pp. 363–391.

YIQI FENG received the M.Eng. degree in mechanical engineering from Beijing Information Science and Technology University, Beijing, China, in 2020. He is currently pursuing the Ph.D. degree with the National Engineering Laboratory for Electric Vehicles, School of Mechanical Engineering, Beijing Institute of Technology. His research interests include permanent magnet synchronous machine drives, stator current predictive control, and data-driven control for AC machine drives.

CHENGNING ZHANG received the M.Eng. degree in control theory and control engineering and the Ph.D. degree in vehicle engineering from Beijing Institute of Technology, Beijing, China, in 1989 and 2001, respectively. He is currently a Professor and the Vice Director of the National Engineering Laboratory for Electric Vehicles, Beijing Institute of Technology. His research interests include electric vehicles, vehicular electric motor drive systems, battery management systems, and chargers.

SHENGPING HUANG received the Master of Engineering degree in transportation engineering from Central South University, in December 2017. He joined Jianglu Machinery Electronics Group Company Ltd., where he is currently a Senior Engineer. His current research interests include vehicle electronics and electrical research.

SHUO ZHANG (Member, IEEE) received the B.Eng. degree from the North China Institute of Aerospace Engineering, Hebei, China, in 2011, and the Ph.D. degree in vehicle engineering from Beijing Institute of Technology, Beijing, China, in 2017.

He is currently an Assistant Professor with the National Engineering Laboratory for Electric Vehicles and the School of Mechanical Engineering, Beijing Institute of Technology. His research interests include the modeling and control of the permanent magnet synchronous motor, multi-motor driving systems, and hybrid power systems.

JIANZHEN QU (Member, IEEE) received the B.Eng. degree from Beijing Forestry University, Beijing, China, in 2014, and the master's and Ph.D. degrees from Beijing Institute of Technology, Beijing, in 2016 and 2021, respectively. From 2018 to 2020, he was with The University of British Columbia as a Visiting Scholar with the Electric Power and Energy Systems Research Group. He is currently a Postdoctoral Research Fellow with the Department of Electrical Engineering, Tsinghua University, Beijing. His research interests include permanent magnet synchronous machine drives condition monitoring, and diagnostics for electric machine drives.

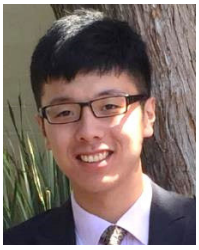

ZHAOZONG LI (Member, IEEE) received the B.E. degree in mechanical engineering from Jilin University, in 2017, and the Ph.D. degree in mechanical engineering from Beijing Institute of Technology, in 2023. He was jointly trained by the Power Electronic Machine and Control Research Group, University of Nottingham, from 2021 to 2022. His research interests include the electromagnetic design and thermal management of advanced electrical machines and electric drive bridges in electrified transportation.

LI ZHAI (Member, IEEE) received the Ph.D. degree in vehicle engineering from Beijing Institute of Technology, Beijing, China, in 2004. From 2009 to 2019, she was an Associate Professor. From 2013 to 2014, she was a Visitor Scholar in electrical and computer engineering with the University of Missouri-Rolla, Rolla, MO, USA. Since 2020, she has been a Professor with the National Engineering Laboratory for Electric Vehicles and the School of Mechanical Engineering, Beijing Institute of Technology. Her research interests include dynamics control, motor drive system control, and EMC of EVs.

YUE ZHAO received the bachelor's degree in vehicle engineering from Shijiazhuang Tiedao University, in 2018. He is currently pursuing the Ph.D. degree with Beijing Institute of Technology. His research interests include robust design and optimization on electrical machines, and torque ripple analysis considering manufacturing tolerances.